European Journal of Medicinal Chemistry 122 (2016) 326–338

Contents lists available at ScienceDirect

European Journal of Medicinal Chemistry

journal homepage: http://www.elsevier.com/locate/ejmech

Research paper

Avarol derivatives as competitive AChE inhibitors, non hepatotoxic and neuroprotective agents for Alzheimer's disease

Giuseppina Tommonaro [a, **], Nuria García-Font [b], Rosa Maria Vitale [a], Boris Pejin [c], Carmine Iodice [a], Sixta Cañadas [b], José Marco-Contelles [d], María Jesús Oset-Gasque [b, *]

[a] Consiglio Nazionale delle Ricerche, Istituto di Chimica Biomolecolare (ICB), Pozzuoli, NA, Italy
[b] Universidad Complutense de Madrid, Facultad de Farmacia, Dpto. de Bioquímica y Biología Molecular II, Spain
[c] University of Belgrade, Department of Life Sciences, Institute for Multidisciplinary Research – IMSI, Belgrade, Serbia
[d] Laboratory of Medicinal Chemistry (IQOG, CSIC), Madrid, Spain

ARTICLE INFO

Article history:
Received 16 February 2016
Received in revised form
2 June 2016
Accepted 19 June 2016
Available online 23 June 2016

Keywords:
Avarol
Thiosalycil-prenyl-hydroquinones (TPHs)
Alzheimer's disease
Anticholinesterasic compounds
Neuroprotection
Molecular modeling

ABSTRACT

Avarol is a marine sesquiterpenoid hydroquinone, previously isolated from the marine sponge *Dysidea avara* Schmidt (Dictyoceratida), with antiinflammatory, antitumor, antioxidant, antiplatelet, anti-HIV, and antipsoriatic effects. Recent findings indicate that some thio-avarol derivatives exhibit acetylcholinesterase (AChE) inhibitory activity. The multiple pharmacological properties of avarol, thio-avarol and/or their derivatives prompted us to continue the *in vitro* screening, focusing on their AChE inhibitory and neuroprotective effects. Due to the complex nature of Alzheimer's disease (AD), there is a renewed search for new, non hepatotoxic anticholinesterasic compounds. This paper describes the synthesis and *in vitro* biological evaluation of avarol-3′-thiosalicylate (**TAVA**) and thiosalycil-prenyl-hydroquinones (**TPHs**), as non hepatotoxic anticholinesterasic agents, showing a good neuroprotective effect on the decreased viability of SHSY5Y human neuroblastoma cells induced by oligomycin A/rotenone and okadaic acid. A molecular modeling study was also undertaken on the most promising molecules within the series to elucidate their AChE binding modes and in particular the role played by the carboxylate group in enzyme inhibition. Among them, **TPH4**, bearing a geranylgeraniol substituent, is the most significant *Electrophorus electricus* AChE (*Ee*AChE) inhibitor (IC_{50} = 6.77 ± 0.24 μM), also endowed with a moderate serum horse butyrylcholinesterase (eqBuChE) inhibitory activity, being also the least hepatotoxic and the best neuroprotective compound of the series. Thus, **TPHs** represents a new family of synthetic compounds, chemically related to the natural compound avarol, which has been discovered for the potential treatment of AD. Findings prove the relevance of **TPHs** as a new possible generation of competitive AChE inhibitors pointing out the importance of the salycilic substituents on the hydroquinone ring. Since these compounds do not belong to the class of alkaloids, which are notorious for their capability to inhibit AChE while exhibiting side effects, they may constitute novel active AChE inhibitors with fewer side effects.

1. Introduction

Alzheimer's disease (AD) is an age-related neurodegenerative disorder, whose prevalence is expected to raise significantly in the next decades, as the average age of the population increases [1]. Worldwide, it is estimated that 40 million people suffer from AD [2]. AD is characterized by a progressive memory loss, a decline in language skills and other cognitive impairments [3]. Although the etiology of AD is not completely known, common hallmarks, such as β-amyloid (Aβ) deposits [4], τ-protein aggregation [5] and oxidative stress [6] are thought to play key roles in the

Abbreviations: ACh, Acetylcholine; Aβ, Amyloid-β peptide; AChE, Acetylcholinesterase; *Ee*AChE, *Electrophorus electricus* AChE; AChEI, AChE inhibitors; ATCh, Acetylthiocholine; AD, Alzheimer's disease; ADME, Absorption, Distribution, Metabolism and Excretion; BuChE, Butyrylcholinesterase; eqBuChE, serum horse BuChE; ChE, Cholinesterases; OKA, Okadaic Acid; PAS, Peripheral Anionic Site; O/R, oligomycin-A/rotenone; ROS, reactive oxygen species; Olig/Rot, oligomycin-A/rotenone; SAR, Structure Activity Relationship; TAVA, avarol-3′-thiosalicylate; TPHs, thiosalycil-prenyl-hydroquinones.

* Corresponding author.
** Corresponding author.
E-mail addresses: gtommonaro@icb.cnr.it (G. Tommonaro), nurilen_12@hotmail.com (N. García-Font), rmvitale@icb.cnr.it (R.M. Vitale), brspjn@gmail.com (B. Pejin), ciodice@icb.cnr.it (C. Iodice), sicada@ucm.es (S. Cañadas), jlmarco@iqog.csic.es (J. Marco-Contelles), mjoset@ucm.es (M.J. Oset-Gasque).

http://dx.doi.org/10.1016/j.ejmech.2016.06.036
0223-5234/

pathophysiology of the disease [7]. In addition, the selective loss of cholinergic neurons in AD results in a deficit of acetylcholine (ACh) in specific brain regions that mediate learning and memory [8]. Alterations in the serotoninergic, and dopaminergic systems are also thought to be responsible for the behavioural disturbances observed in AD patients [9].

At present, there are three FDA-approved drugs (donepezil, galantamine and rivastigmine) [10] that aim to improve AD symptoms by inhibiting acetylcholinesterase (AChE), the enzyme responsible for the hydrolysis of ACh, thus raising the ACh content in the synapsis [11]. Apart from the beneficial palliative properties of AChE inhibitors (AChEI) in AD, cholinergic drugs have shown little efficacy to prevent the progression of the disease. Consequently, nowadays there is no efficient therapy to cure, stop or even slow the progression of the disease, and therefore, effective therapeutics are urgently sought [12].

Avarol and avarone (Fig. 1), two sesquiterpenes bearing a hydroquinone and quinone functional motif, respectively, possessing a rearranged drimane skeleton, have been isolated from the marine sponge *Dysidea avara* Schimdt [13]. Previous studies have revealed that these secondary metabolites show a wide variety of biological activities, such as antibacterial, antifungal, antiviral, cytotoxic, antioxidant, anti-inflammatory and anti-psoriatic effects [14]. Some previous biological studies on different derivatives of avarol, involving both the aromatic ring and sesquiterpenoid moiety, revealed that the terpenoid moiety plays a marginal role in biological processes, while the hydroquinone/quinone couple is the main group responsible for the observed biological activity [15,16]. Recent findings indicate that some thio-avarol derivatives exhibit AChE inhibitory activity [17,18]. The multiple pharmacological properties of avarol, avarone and/or their derivatives prompted us to continue with the *in vitro* screening of the bioactivity noted, focusing on their AChE inhibitory effect and its potential neuroprotective effect. Starting from the scaffold already explored in previous studies [18] we considered new compounds by easy, cheap and fast synthesis, keeping the main functional groups, such as the hydroquinone ring substituted with thiosalicylic acid in position 3′, and changing the drimane moiety into a linear terpenoid chain bearing from one to four isoprene units (from C5 up to C20). In this way, the new compounds leave aside from the availability of natural source, the marine sponge, from which to extract avarol and on which to perform the chemical derivatization. Moreover, a molecular modeling study was undertaken on the most active AChE inhibitors to determine their binding modes toward the enzyme and to explain the role played by the negatively charged moiety, rather unusual among known AChE inhibitors. Since thiosalycil-prenyl-hydroquinones (**TPHs**) exhibit features very different from the class of alkaloids, which are notorious for their capability to inhibit AChE while exhibiting side effects, these compounds may constitute novel active AChE chemicals with fewer side effects.

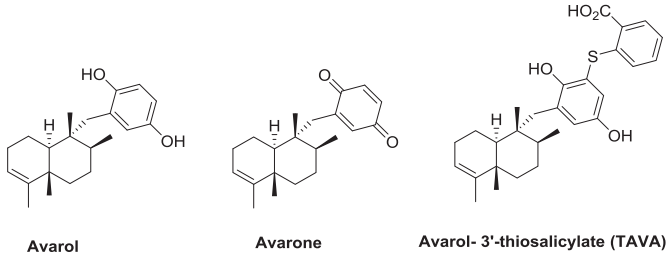

Fig. 1. Chemical structures of avarol, avarone and avarol- 3′-thiosalicylate (**TAVA**).

2. Results and discussion

2.1. Chemistry

Avarol (Fig. 1), a natural sesquiterpenoid hydroquinone isolated from the marine sponge *D. avara*, exhibited several biological activities [19–21]. The interesting properties of avarol and the previous findings that avarone, the quinone of avarol (Fig. 1), reacts against protein sulfhydryl groups prompted researchers to prepare several sulfhydryl derivatives of avarol and to extend the evaluation to other biological properties [16,17,22]. The main difficulty of the application of the mentioned avarol derivatives is related to ecological feature that is the continuous availability of natural source, the marine sponge. Accordingly, a series of **TPHs**, containing isoprene groups from 5 up to 20 carbons in length (**TPH1-5**, Scheme 1) were synthesized as structural analogs of avarol- 3′-thiosalicylate (**TAVA**) (Fig. 1), and tested for their AChE inhibitory effect.

The **TPHs** were synthesized according very easy and fast reactions, in two simple steps: 1) addition of the allylic alcohol (3-methyl-2-buten-1-ol or geraniol or farnesol or phytol or geranylgeraniol) to the acidic solution of hydroquinone, in anhydrous media to obtain prenyl-hydroquinones (Scheme 1); 2) addition of thiosalicylic acid to a solution of oxidated form of avarol (avarone) in ethanol to obtain thiosalycil prenyl-hydroquinones (TPHs) (Scheme 1). All compounds were identified by comparison of their spectral data with those reported in the previous literature [23]. The position of the substituent was also determined by the analysis of ^{1}H and ^{13}C NMR spectra (see Experimental Section).

2.2. In vitro AChE and BuChE inhibitory activity

Next, we addressed the capacity of these **TPHs** to inhibit *Ee*AChE and eqBuChE by using the Ellman's method, and tacrine and galantamine as standards for comparative purposes [24]. As shown in Table 1, **TPH1-5** and **TAVA** are moderate *Ee*AChEI, from low to high micromolar range, most of them showing statistically significant higher IC_{50} values than galantamine or tacrine. However, **TAVA** has a significantly lower IC_{50} value than avarol. Among the synthetic TPHs, **TPH4** showed the most significant AChEI activity (IC_{50} = 6.77 ± 0.24 μM), this compound bearing a geranylgeraniol substituent and showing a similar inhibition profile similar to **TPH1** and even better than **TAVA** and the other **TPH** compounds (Table 1).

We also tested the inhibition of eqBuChE, by **TPH1-5** using the Ellman's method [24], and tacrine as standard, since galantamine is not a BuChEI. The observed results are shown in Table 1. From these results we could infer that while the avarol is poorly active/inactive, both **TAVA** and two of **TPH** derivatives, **TPHs 4** and **5** porting a geranylgeraniol or phytol substituent, respectively, exhibit a moderate BuChE inhibitory activity, with IC_{50} values very similar between **TAVA** and **TPHs 4** and **5**. **TPH5** was the most potent BuChEI since it showed a roughly 95% enzymatic inhibition at 50 μM.

Thus, we conclude that both **TAVA** and **TPHs 4** and **5** exhibit good AChE and moderate BuChE inhibitory activity, particularly **TPHs 4** and **5** being the most potent *Ee*AChEI and eqBuChEI, respectively.

2.3. Kinetic analysis of inhibition of EeAChE

Next and based on these results we analyzed the kinetic *Ee*AChE inhibitory mechanism by **TAVA** and **TPHs 1** and **4**, as the most potent AChEI among all tested compounds. As shown in Fig. 2 and Table 2, the graphical double-reciprocal analysis of Lineweaver–Burk for all of these compounds shows a statistically

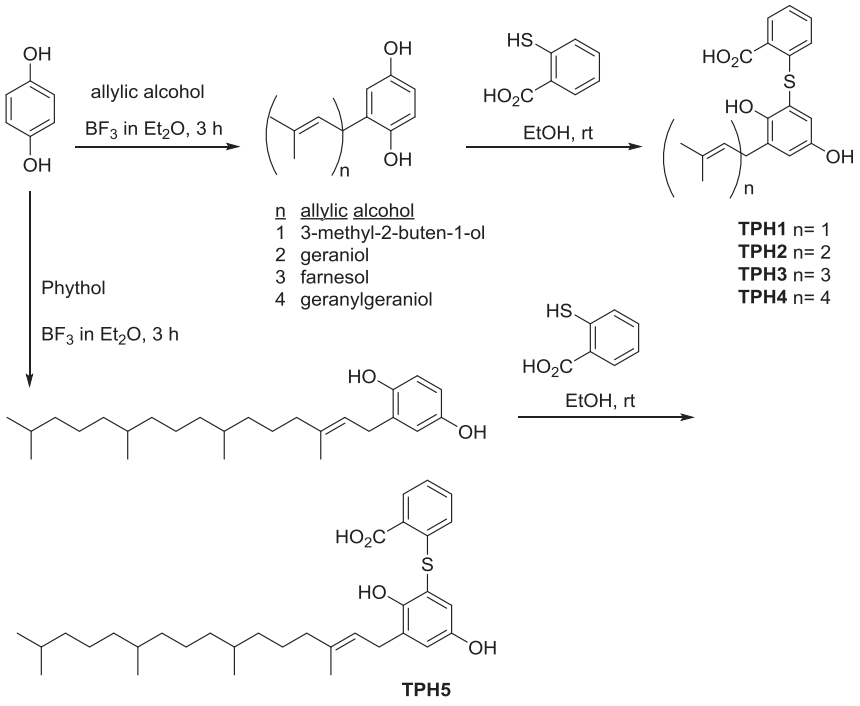

Scheme 1. Synthesis of 3′-thiosalycil prenylhydroquinones **1**–**5**.

Table 1
Inhibition of EeAChE and eqBuChE by **TPHs 1**–**5** and **TAVA**.

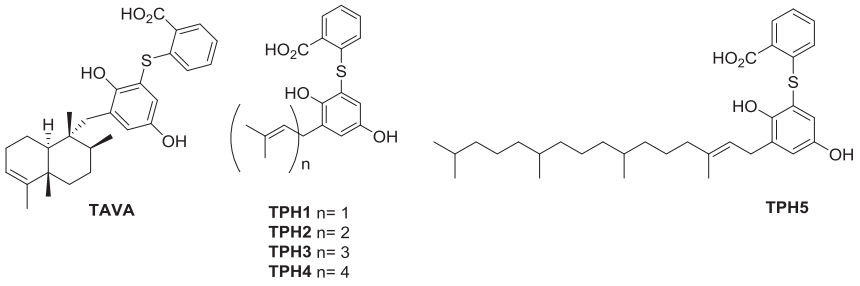

Compound	EeAChE activity IC_{50} ± SEM (μM)	P < GAL	P < TAVA	BuChE activity		P < TAC	P < TAVA
				Maximal inhibition (%)/(Conc.)	IC_{50} ± SEM (μM)		
Tacrine	0.061 ± 0.0012	–	***	100 (10 μM)	0.0012 ± 0.00006	–	–
Galantamine	0.61 ± 0.07	–	***	nd	–	–	–
Avarol	285.63 ± 43.50	***	***	3.3 (10 μM)	NC	***	***
TAVA	15.11 ± 2.90	***	–	77.5 (50 μM)	15.14 ± 3.20	***	–
TPH1	7.88 ± 1.80	***	*	13.1 (50 μM)	NC	***	***
TPH2	13.09 ± 2.60	***	ns	17.8 (50 μM)	NC	***	***
TPH3	18.10 ± 1.99	***	ns	8.4 (50 μM)	NC	***	***
TPH4	6.77 ± 0.24	***	**	60.5 (50 μM)	19.70 ± 5.25	***	ns
TPH5	13.79 ± 2.50	***	ns	94.3 (50 μM)	12.85 ± 4.80	***	ns

Values are expressed as mean ± sem of at least three different experiments in duplicate; ***P < 0.001, **P < 0.01, *P < 0.05 and ns non significant, with respect to galantamine (GAL), tacrine (TAC) or TAVA. Comparisons between drugs were performed by one-way ANOVA test. (NC = non-calculated).

significant increase in origin abscissas [1/I] without significantly affecting the slopes or the origin ordinates (1/Vmax), which indicates that the three compounds behave as competitive inhibitors. These results were confirmed by the statistical analysis of Km and Vmax tendencies (Table 2), which clearly shows a significant tendency for Km to increase while Vmax does not exhibit such tendency.

These results clearly show that all assayed compounds (**TAVA**, **TPHs 1** and **4**) exhibit a competitive inhibition profile, as confirmed by molecular modeling (see below), which could be further extended to the other members of the **TPH** family. However, at concentrations higher than 10 μM, **TPH4** showed a mixed profile as AChEI, since a decrease in Vmax was additionally shown. The Dixon analysis (plot of Km at different compound concentrations) allowed for an estimation of Ki of 0.0585 ± 0.037 nM, 0.221 ± 0.049 nM and 0.00059 ± 0.00005 nM ($p < 0.01$ ANOVA, $n = 3$) for **TAVA**, **TPH1** and

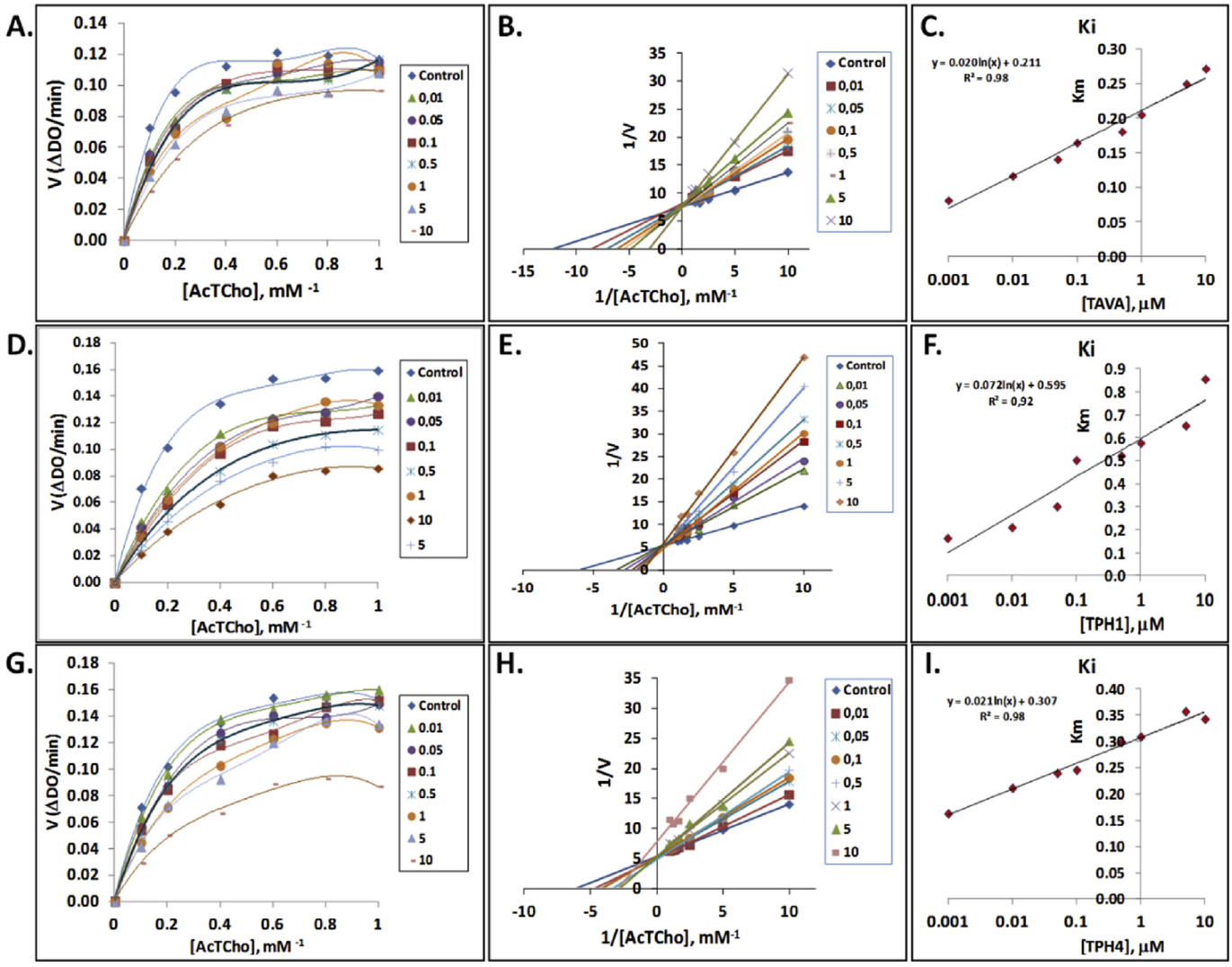

Fig. 2. Kinetics of the inhibition of *Ee*AChE by **TAVA** (A-C), **TPH1** (D-F) and **TPH4** (G-I), at concentrations between 0.001 and 10 µM, according to Michaelis-Menten (A,D,G); according to Lineweaver-Burk (B, E, H) and determination of Ki (Dixon) (C, F, I).

Table 2
Mechanism of inhibition of *Ee*AChE by **TAVA**, **TPHs 1** and **4**.

[Comp.] µM	TAVA		TPH1		TPH4	
	Km (µM)	Vmax (ΔDO/min)	Km (µM)	Vmax (ΔDO/min)	Km (µM)	Vmax (ΔDO/min)
Control	0.103 ± 0.022	0.133 ± 0.021	0.153 ± 0.027	0.178 ± 0.033	0.162 ± 0.021	0.186 ± 0.016
0.01	0.116 ± 0.031	0.123 ± 0.030	0.295 ± 0.034***	0.181 ± 0.021	0.211 ± 0.024	0.198 ± 0.034
0.05	0.142 ± 0.017	0.131 ± 0.035	0.356 ± 0.029***	0.186 ± 0.015	0.239 ± 0.030	0.190 ± 0.027
0.1	0.164 ± 0.028	0.135 ± 0.024	0.452 ± 0.032***	0.194 ± 0.021	0.245 ± 0.027	0.187 ± 0.031
0.5	0.181 ± 0.014*	0.135 ± 0.030	0.522 ± 0.024***	0.188 ± 0.019	0.299 ± 0.032**	0.205 ± 0.024
1	0.205 ± 0.026*	0.136 ± 0.016	0.542 ± 0.064***	0.120 ± 0.031	0.309 ± 0.029**	0.181 ± 0.028
5	0.210 ± 0.03**	0.127 ± 0.021	0.653 ± 0.052***	0.188 ± 0.022	0.357 ± 0.031***	0.188 ± 0.019
10	0.321 ± 0.05***	0.135 ± 0.018	0.697 ± 0.071***	0.170 ± 0.019	0.343 ± 0.039***	0.129 ± 0.017

Values expressed as mean ± standard error of the mean of three different experiments in duplicate; ns = no significant. ***P < 0.001., **P < 0.01, *P < 0.05 with respect to control (one-way ANOVA test).

TPH4, respectively (Fig. 2C, F, I), which shows that affinity of **TPH4** for enzyme is about 100 and 375 folds higher than that of **TAVA** and **TPH1**, respectively. These differences, together with their different BuChE inhibitory activity, could probably explain the different neuroprotective activity observed for these compounds (see below) and thus, justify that **TPH4** exhibit the stronger neuroprotective capacity.

2.4. Neuroprotection studies

2.4.1. Oligomycin A/Rotenone

Based on these results, we next addressed the analysis of the neuroprotective capacity of **TAVA** and **TPHs 4** and **5**. We selected the cocktail Oligomycin A (10 µM)/Rotenone (30 µM) (OR) as the toxic insult, which blocks the mitochondrial electron transport

chain complexes I and V, respectively, thus inducing cell death by oxidative stress in a concentration-dependent manner. Neuroprotection studies were carried out at different concentrations, between 0.1 and 100 μM, in order to determine the (%) maximum cell viability, and the neuroprotective EC_{50} values. For this analysis, the difference in viability between the control and the mixture OR was used as 100% neuroprotection (see Experimental Section).

In these experiments galantamine was used as a positive control, because it is known than this compound is a cholinergic drug with antioxidant and neuroprotective properties linked to its inhibition of acetylcholinesterase and allosteric modulation of nicotinic receptors. In SHSY5Y cells, it was found that galantamine afford neuroprotection against respiratory chain inhibition [25]. In our experiments galantamine showed a good neuroprotective effect with an $EC_{50} = 2.81 \pm 0.25$ μM (Fig. 3). This effect is very similar to that found for its neuroprotective effect against NMDA-induced excitotoxicity in cultures neurons (EC_{50} = 1.48 μM) [26], and it could be due to its anticholinesterasic effect and its effect as a modulator of the α7 and β2 nAChRs expressed in SHSY5Y neuroblastoma cells [27].

In Fig. 3A and B, curves the % of neuroprotection against OR of different compounds at the indicated concentrations (A), and EC_{50} values (B) are shown. As shown in this figure, at these concentrations, although all compounds exhibited EC_{50} in the range of lower μM, **TPH4** ($EC_{50} = 0.52 \pm 0.15$ μM) showed the strongest neuroprotective effect, higher than galantamine used as positive control and similar to **TAVA**. From these results a clear structure-activity relationship could be deduced. Thus in the case of **TPH1-3** compounds, the longer the isoprenyl chain number units of these compounds is, the lower their neuroprotective capacity. However, **TPHs 4** and **5** compounds are better neuroprotective compounds than those with shorter isoprene chains. This indicates that the longer the isoprenyl unit length of the compounds, the better their interaction with the enzyme and thus, their better neuroprotective abilities.

2.4.2. Okadaic acid

In order to gain a deeper insight into the neuroprotective capacity of **TAVA** and **TPHs 4** and **5**, and given that one of the most relevant molecular changes in AD is tau-hyperphosphorylation, we next assessed the ability of these molecules to prevent cell death mediated by okadaic acid (OKA), which is known to actívate tau phosphorylation. At 20 nM OKA (concentration at which it decrease cell viability at 40–60%) it was able to significantly increase GSK-3β phosphorylation at ^{216}Tyr, as well as at tau ^{396}Ser (24). Next, and consequently, the neuroprotective effect of 0.01–50 μM concentrations of these compounds, on cell death induced by 20 nM OKA, was analyzed.

In this case galantamine showed a good neuroprotective effect too, with an $EC_{50} = 1.94 \pm 0.09$ μM (Fig. 4). This effect is also very similar to that found for its neuroprotective effect against O/R (this paper) and against NMDA-induced excitotoxicity in cultured cortical neurons [26].

Results in Fig. 4 demonstrate that all **TPHs** were good neuroprotective agents against OKA-induced cell death. However, **TPH4** was again the most potent compound at reverting the cell death induced by OKA at 20 nM. The fact that **TPH5** is not as potent a neuroprotector as **TPH4** against cell death induced by OKA, even if both compounds are equipotent at reverting cell death induced by OR, means that the group geranylgeraniol adds a very high level of neuroprotection to these TPH compounds, with **TPH4** being, together with **TPH2**, the most potent compound against cell death induced by tau phosphorylation. Thus, these compounds, of which **TPH4** showed a 20 times lower EC_{50} than **TAVA** (0.15 ± 0.03 μM against 3.35 ± 0.2 μM, respectively), could be the most efficient compound as neuroprotector in AD. In Fig. 5 we have inserted images showing the neuroprotective effects of **TPH4** and **TAVA** against cell death mediated by OKA at 20 nM and O10/R30 μM. Note that in the both conditions, **TPH4** and **TAVA** are very efficient neuroprotectors with a very similar potency between them.

Aβ-aggregation together with tau phosphorylation are considered as two of the most important events in the cascade of molecular alterations leading to AD. In addition, Aβ has been proposed as an allosteric modulator of the intrinsic catalytic efficiency of ChEs, thereby regulating the synaptic and extrasynaptic cholinergic signaling [28]. Our preliminary results with $A\beta_{1\text{-}40}$, which causes 41 ± 4.5% cell death at 20 μM, show that these compounds were not able to revert this effect (data not shown). Thus, these results are in agreement with the competitive nature of the AChEI properties of these compounds and their inability to bind with W286 into the PAS site of the enzyme (see below), the main residue involved in AChE-induced fibrillation, a requisite which could be important to displace Aβ from its binding site to the enzyme [29,30].

Due to the fact that the neuroprotective effects of some of these

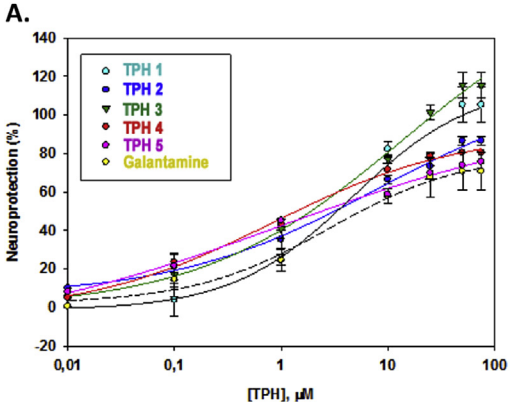

B.

Compound	EC_{50} (μM)	P< (Gal)	P< (TPH 4)	P< (TAVA)
TPH 1	4.65 ± 0.58	ns	*	*
TPH 2	8.17 ± 1.44	**	***	***
TPH 3	13.60 ± 2.17	***	***	***
TPH 4	0.52 ± 0.06	ns	-	ns
TPH 5	1.1 ± 0.16	ns	ns	*
Galantamine	2.81 ± 0.25	-	ns	*
TAVA	0.21 ± 0.03	*	ns	-

Fig. 3. Neuroprotective effects of **TAVA** and **TPH** compounds against cell death induced by 10 μM oligomycine/30 μM rotenone (OR) in SHSY5Y neuroblastoma cells. (**A**) Dose-response curves showing the (%) neuroprotection of different compounds at the indicated concentrations. The curve adjustments to estimate the EC_{50} were carried out by non-linear ponderated regression analysis of minimal squared, using logistic curves f1 = min + (max-min)/(1 + (x/IC_{50})$^{-}$(-Hillslope). Data represent mean ± SEM of three experiments, each one done in triplicate (n = 9). The analysis was implemented using the software SigmaPlot v.11. (**B**) EC_{50} values for the indicated compounds. The statistics compares the differences between EC_{50} values for different compounds tested against galantamine, **TPH4** or **TAVA** at *P < 0.05, **P < 0.01 y ***P < 0.001 (ANOVA one way).

A.

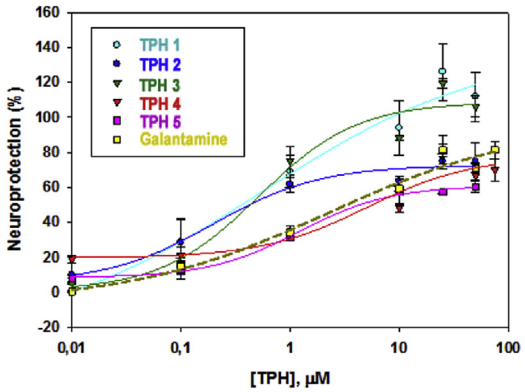

B.

Compound	EC_{50} (μM)	P< (Gal)	P< (TPH 4)	P< (TAVA)
TPH 1	0.54 ± 0.08	***	**	***
TPH 2	0.22 ± 0.02	***	ns	***
TPH 3	0.516 ± 0.05	***	***	***
TPH 4	0.15 ± 0.03	***	-	***
TPH 5	1.21 ± 0.03	***	***	***
Galantamine	1.94 ± 0.09	-	***	***
TAVA	3.35 ± 0.20	***	***	-

Fig. 4. Neuroprotective effects of **TAVA** and **TPH** compounds against cell death induced by 20 nM OKA in SHSY5Y neuroblastoma cells. (A-B) Dose-response curves showing the (%) neuroprotection of different compounds at the indicated concentrations. The curve adjustments to estimate the EC_{50} were carried out by non-linear ponderated regression analysis of minimal squared, using logistic curves f1 = min + (max-min)/(1 + (x/IC_{50})^(-Hillslope). Data represent mean ± SEM of three experiments, each one done in triplicate (n = 9). The analysis was implemented using the software SigmaPlot v.11. (**B**) EC_{50} values for the indicated compounds. The statistics compares the differences between EC_{50} values for different compounds tested against galantamine, **TPH4** or **TAVA** at *P < 0.05, **P < 0.01 y ***P < 0.001 (ANOVA one way).

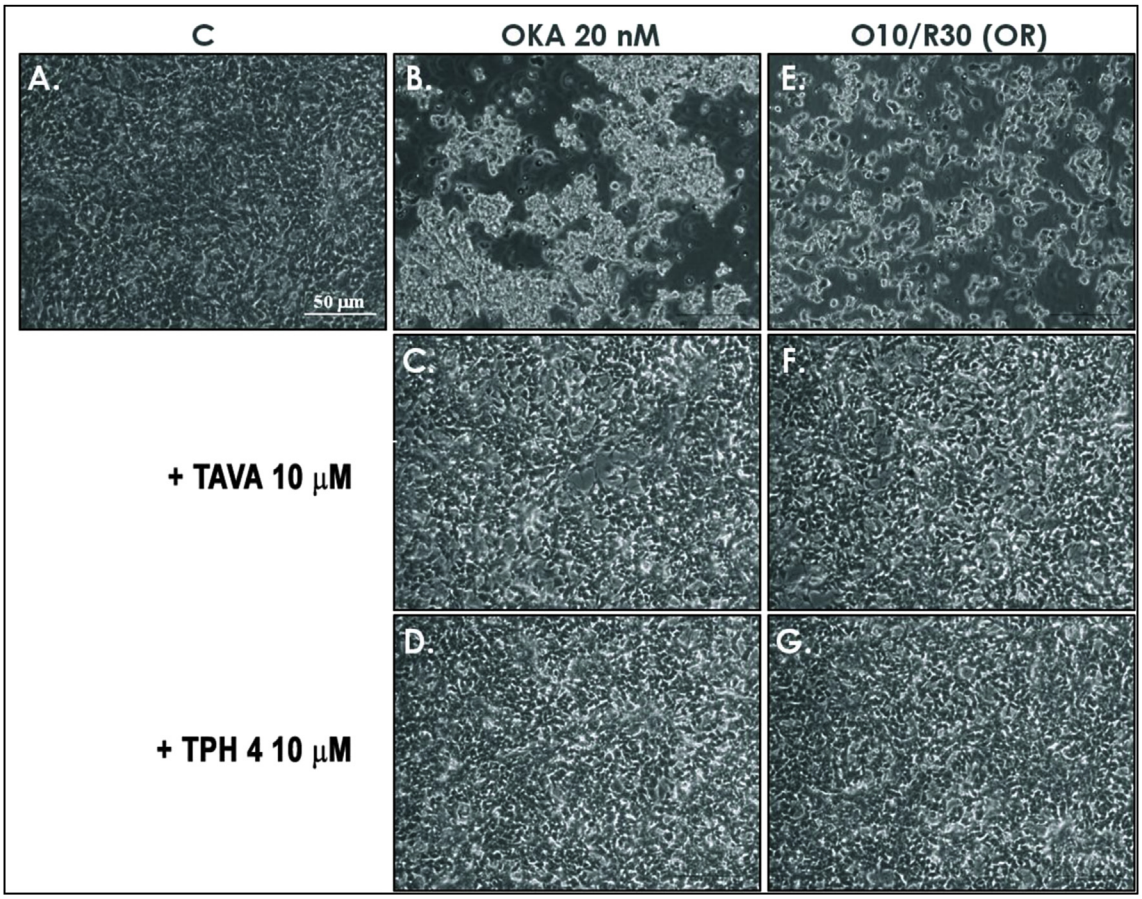

Fig. 5. Neuroprotective effects of **TAVA** and **TPH4** against cell death induced by OKA and OR in SHSY5Y neuroblastoma cells. Phase contrast microscopy images showing the neuroprotective effects of 10 μM **TAVA** and **TPH4** against the cell death mediated by OKA at 20 nM (B-D) or OR (E-G). C, control. Scale bar = 50 μm.

compounds decrease at ≥50–100 μM, we evaluated their basal neurotoxicity. Unlike the toxic effects shown by tacrine (>25–60% at 25 μM) [31], avarol-derived compounds proved to be, similarly to galantamine, non-neurotoxic compounds between 1 and 25–50 μM concentrations (Fig. 6).

2.5. Hepatotoxicity study

Given that anticholinesterasic compounds for AD treatment, like tacrine, exhibited hepatotoxicity via elevation of serum alanine aminotransferase levels and thus showed limited clinical application and in consequence were withdrawn from the pharmaceutical

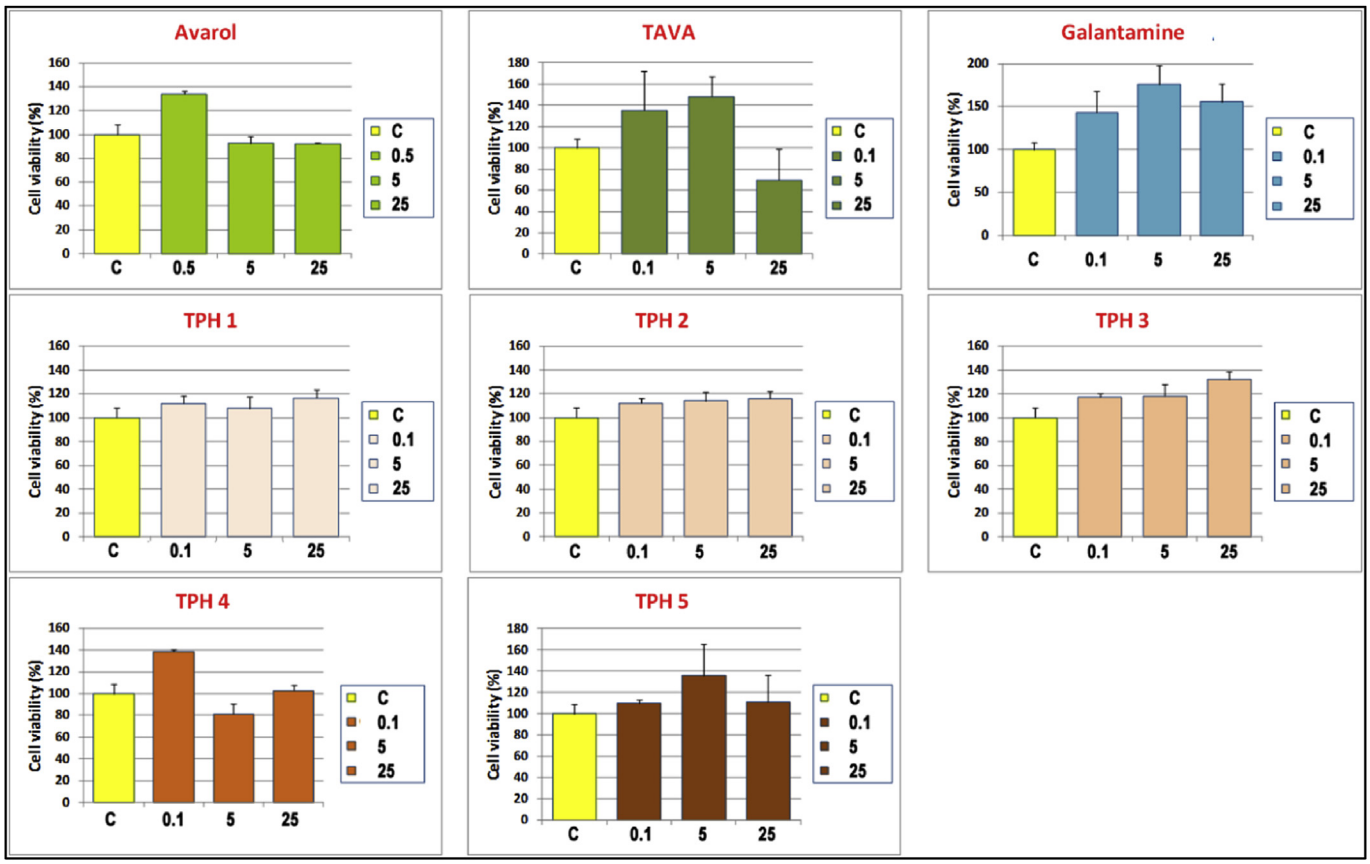

Fig. 6. Neurotoxic effect of avarol-derivatives, **TPHs** and galantamine on the cellular viability of SHSY5Y neuroblastoma cells in culture. Results represent the % of cellular viability in the presence, or lack (control; C) of different concentrations of the indicated compounds. The values are the mean ± SEM of at least three independent experiments, each one carried out in triplicate, in different cultures. The statistical analysis shows the neurotoxic or neuroprotective effects against controls at $^{*}P < 0.05$, $^{**}P < 0.01$, $^{***}P < 0.001$ (one way ANOVA).

market shortly after its approval, a very critical point for AChEI to be considered as gold standard for AD drug discovery is that they did not present hepatotoxicity. For this reason, we investigated the hepatotoxicity of avarol, **TAVA** and **TPH** compounds, on HepG2 cells, in a concentration range of 1–100 μM HepG2 cells are considered as a useful model to study *in vitro* xenobiotic metabolism and liver toxicity. In particular, HepG2 cells are able to activate and detoxify xenobiotics and they are utilised to study the mechanism of action of drugs [32]. Compounds hepatotoxicity was determined using the XTT assay. These compounds were well tolerated after a 24 h incubation period in human HepG2 cells compared with tacrine, as shown in Fig. 7.

The hepatotoxicity of tacrine (64.3 ± 4.54: $P < 0.001$, Anova test, at 100 μM) [31] is associated with increased levels of intracellular reactive oxygen species (ROS) and decreased level of antioxidant defenses [33,34]. As shown in Fig. 7, the most hepatotoxic compound was **TAVA** which decreases the number of living cells at the low concentration of 50 μM, being more hepatotoxic gradually at increasing doses. It is worth mentioning that avarol and **TPHs 1**–**4** are not hepatotoxic at all and that **TPH5** at the highest concentration used (100 μM) showed a reduced hepatotoxicity compared with **TAVA**. In special **TPH4** was shown not to be hepatotoxic at all. In fact, it was found to afford hepatoprotection at concentrations ranging from 1 to 25 μM. Thus, these **TPH** compounds exhibited a wide therapeutical safety range.

Thus, it seem clear that the substitution by a geranylgeraniol in the hydroquinone ring motif in avarol, coupled with a suitable selection of the substituents at defined and synthetically available aromatic positions, produces new compounds devoid of the toxic effects present in the reference compound.

2.6. Molecular modeling [35–50]

A combined approach of molecular docking and molecular dynamics simulations was undertaken to investigate the binding modes of the most actives compounds among the terpenoid series, i.e. **TPH1** and **TPH4**, along with **TAVA**. All compounds, after an initial rearrangement of the terpenoid side chain, give stable binding modes during MD simulation (Fig. 8). **TPH4** gave rise to the deeper rearrangement, stabilizing in the last 10 ns These ligands share a similar binding pose of the hydroquinone-thiosalicylic acid moiety (Fig. 9), which in all complexes is positioned in the Catalytic Anionic Site (CAS) and engages a stable H-bond (occurrence during MD > 90%) between its carboxylate group and the catalytic Ser202 hAChE S203. This interaction fully explains the competitive binding modes observed experimentally. In all three simulated complexes a resident water molecule occurs, bridging the ligand carboxylate group to the amide backbone of the residues forming the oxyanion hole (Gly120 (hAChE G121), Gly121 (hAChE G122) and Ala203 (hAChE A204)). In the case of **TPH1** complex (Fig. 9-a), another water molecule is located between the carboxylate moieties of the ligand and Glu201. The ligand carboxylate group in the CAS is further stabilized by the ionic interaction with Arg236, a residue not conserved in neither human nor torpedo AChE, where it is replaced by Ala237 and Ala234, respectively. The ligand benzylic ring forms π-π stacking interaction with Phe333 (hAChE F338). The hydroxyl groups of the hydroquinone ring of QH5 ligand engage H-bonds with Ser124 (hAChE S125) (~36%), Tyr332 (hAChE Y337)

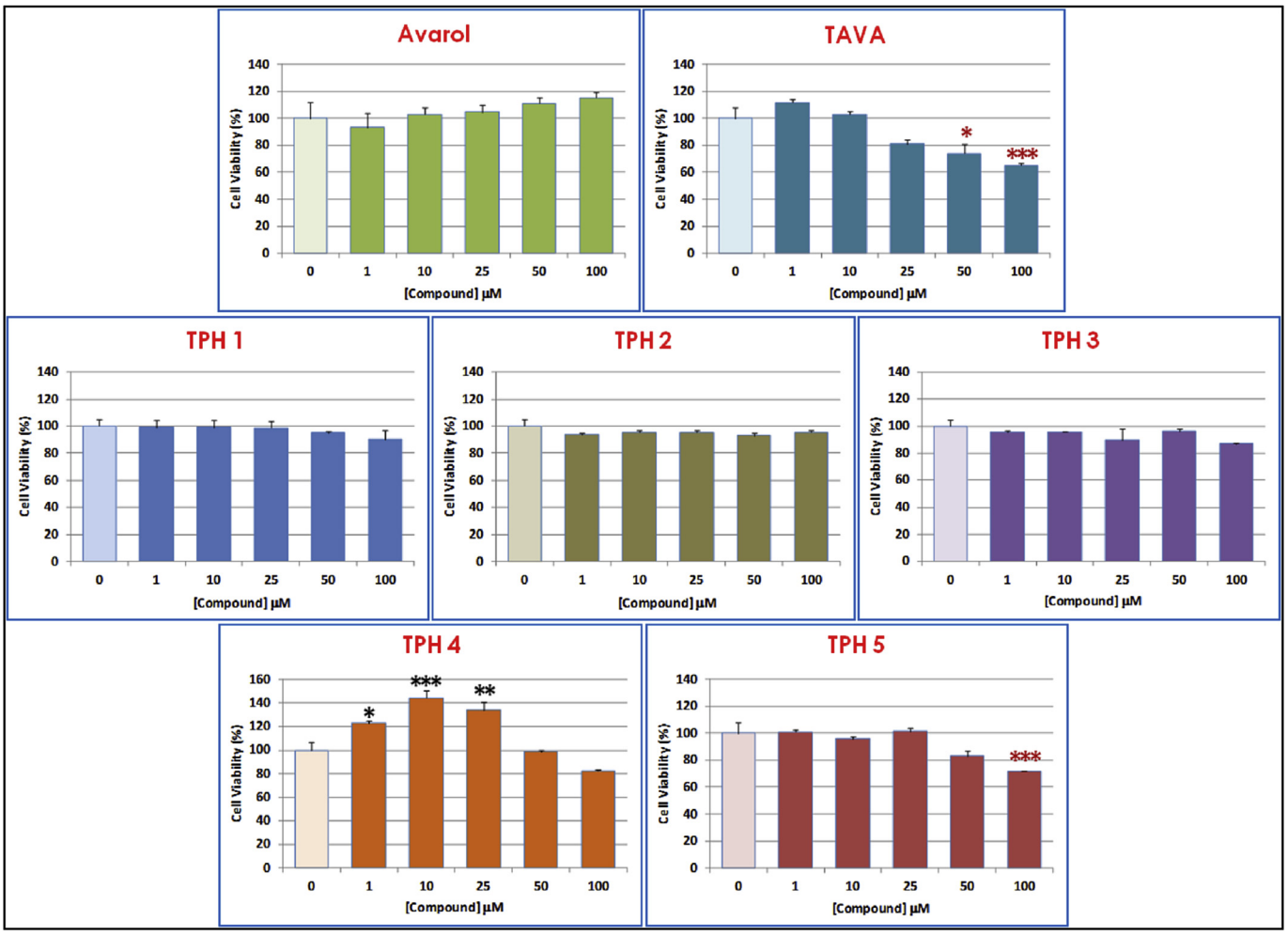

Fig. 7. In vitro hepatotoxicity of avarol-derivatives and **TPHs** in HepG2 cells. Cell viability was measured as XTT reduction and data were normalized as % control. Data are expressed as the means ± s.e.m. of triplicate of at least three different cultures. All compounds were assayed at increasing concentrations (1–100 µM) ***P < 0.001, **P < 0.01, *P < 0.05, with respect to control group (one-way ANOVA test).

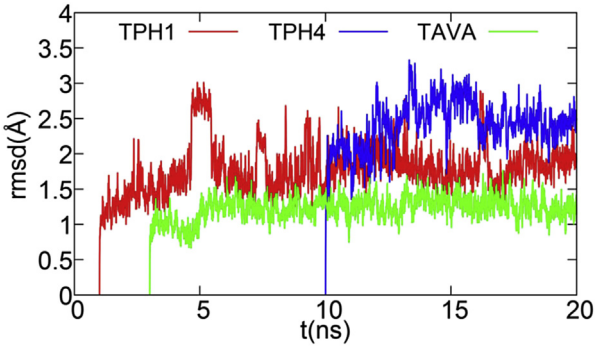

Fig. 8. Root mean square deviation plots for the MD trajectories of *Ee*AChE complexes. Plots are shown for complexes involving the hydroquinone-thiosalicylate derivatives bringing **TPH1** (red, last 19 ns), **TPH4** (blue, last 10 ns) or TAVA (green, last 17 ns) substituents. Rmsd was calculated on backbone atoms of the whole simulated protein sequence and was smoothed by 5-frames moving average. (For interpretation of the references to color in this figure legend, the reader is referred to the web version of this article.)

(~25%) and Tyr123 (hAChE Y124)(~12%), while the terpenoid chain is sandwiched between Tyr336 (hAChE Y341) and Tyr123(hAChE Y124), forming π-π stacking interactions. In **TPH4** (Fig. 9-b), the hydroxyl groups also engages H-bonds with Ser124(hAChE S125) (~23%) and Tyr332 (hAChE Y337)(~10%) while the terpenoid chain is located in the Peripheral Binding Site (PAS), where it stably occupies the cleft between the loop and the helix bearing Trp281 (hAChE W286), although not directly interacting with this latter residue, important for the inhibition of Aβ fibrillation. Here it forms both hydrophobic and π-π interactions with the cluster of aromatic residues of the PAS and the middle gorge region. In this view, the long terpenoid chain of the **TPH4**, although surely paying a high entropic cost for its immobilization upon binding, provides a more than compensating enthalpic stabilization mainly arising from interactions with the aforementioned cleft in comparison with **TPH1** and, especially, **TPHs 2** and **3**. For these two latter compounds, in fact, the shorter length of their isoprenic chain in comparison to **TPH4** could prevent the reaching of the cleft and the adverse entropic contribute, not fully compensated by stable ligand-protein interactions involving their terpenoid chains, may explain their observed lower activities in comparison with both **TPHs 1** and **4**. In the avarol derivative (Fig. 9-c), the policyclic moiety mainly interacts with Phe290 (hAChE F295) and Phe292 (h AChE F297) residues in the acyl pocket, and with Tyr336 (hAChE Y341), whereas, differently from **TPH1** and **TPH4** ligands, the hydroxyl groups of hydroquinone group engage H-bonds with Tyr336 (hAChE Y341) (~20%) and Asp73 (hAChE D74) (~14%). The lower activity of **TAVA** derivative respect to **TPHs 1** and **4** could be ascribed to the less

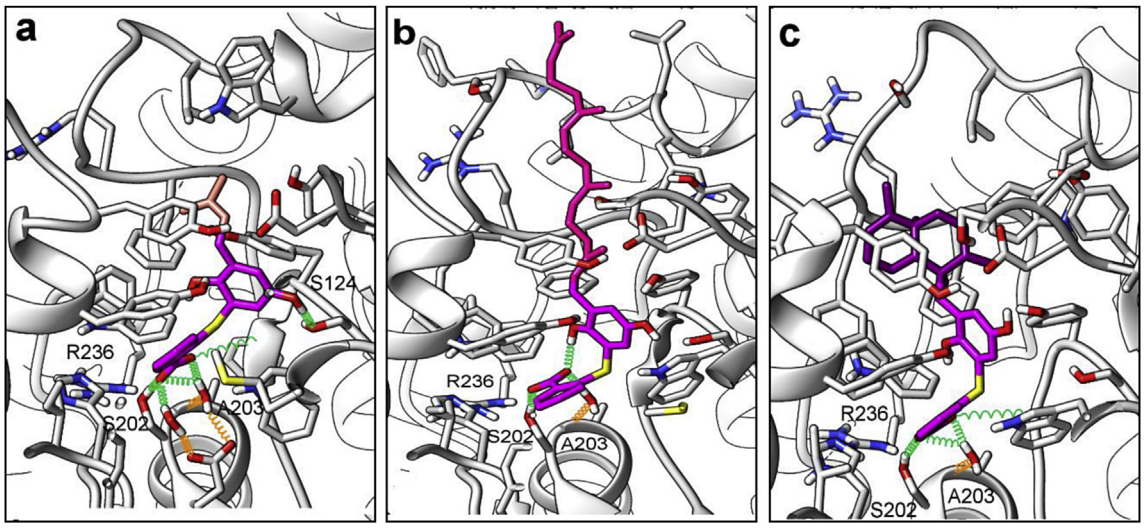

Fig. 9. Protein-ligand interactions in modeled complexes of *Ee*AChE with compounds bringing **TPH1** (a), **TPH4** (b) or **TAVA** (c) substituents. The protein-ligand contact region is shown using a ribbon representation for AChE plus stick sidechain for AChE residues within 5 Å from the ligand and a stick representation for ligands and protein-ligand bridging water molecules. Only polar hydrogens are shown. Carbon atoms are painted white for protein, magenta for the common hydroquinone-thiosalicylate scaffold of the three ligands and light pink, deep pink and dark magenta for **TPHs 1**, **4** and **TAVA** groups, respectively. Nitrogen, oxygen, sulfur and hydrogen atoms are painted blue, red, yellow and white, respectively. H-bonds are represented as green (protein-ligand and water-ligand) or orange (water-protein) springs. (For interpretation of the references to color in this figure legend, the reader is referred to the web version of this article.)

electrophilic nature of the avarol moiety, resulting in the lost of the π-π interactions characteristic of the complexes of the **TPHs 1**/**4**, and/or to the differential desolvation effects upon binding between **TPHs 1**/**4** (whose H-bond partners Ser124 (hAChE S125) and Tyr332 (hAChE Y337) are solvent-exposed in the absence of ligands) and **TAVA** (whose H-bond partners Tyr336 (hACHe Y341) and Asp73 (hAChE D74) are H-bonded each other in the unligated protein).

3. Conclusion

In this work we have reported the synthesis and the *in vitro* biological evaluation of five new **TPHs** as non-hepatotoxic, and neuroprotective anticholinesterasic drugs for the treatment of AD [51]. The competitive inhibition mode of AChE was explained by molecular modeling studies, which showed that the thiosalicylic moiety is able to engage through the carboxylate moiety direct H-bond with the catalytic serine and water-mediated H-bonds with other residues within the oxyanion hole. Thus, the unusual carboxylate moiety for this kind of inhibitors plays a critical role in the inhibitory mechanism, explaining the activity of these acidic derivatives in comparison with avarol.

Among them, **TPH4** is significantly less hepatotoxic than avarol, the parent natural compound, showing increased AChEI and BuChEI activity of competitive-type with IC_{50} values in the low micromolar range. Moreover, this compound has a very good neuroprotective profile not only against O/R but also against OKA, which means that it is not only able to inhibit oxidative stress but also tau phosphorylation and thus it fulfill the requirements to be considered as good multi-target ligand for the potential use as AD therapeutics. The fact that **TAVA** and **TPHs** are endowed with both good inhibitory activity on AChE and moderate activity on BuChE, is very interesting since it has been demonstrated that BuChE is found in neurons and glial cells, as well as in neuritic plaques and tangles in AD patients. In addition, AChE activity decreases progressively in the brain of AD patients, whereas BuChE activity shows some increase, this suggesting that it may replace AChE in the hydrolysis of brain ACh. Therefore, the increase in ACh levels, consequent to the inhibitory capacity of these compounds against both types of cholinesterase (ChE) could be the first step that subsequently drives the inhibition of tau oligomerization and phosphorylation, which would in turn trigger the progression of AD.

To sum up, new avarol derivatives, such as **TAVA** and **TPH4**, the best AChEI and BuChEI, respectively, showing no hepatotoxic and neurotoxic properties, are remarkable neuroprotectors against cell death induced by oxidative stress as well as τ-phosphorylation and aggregation. Therefore, they fulfill the requirements to be considered as the best multi target ligand found in this work for the potential use as AD therapeutics [52,53].

4. Experimental Section

4.1. Synthesis of thiosalicylate prenylhydroquinones (TPHs) and avarol- 3′-thiosalicylate (TAVA)

The synthesis of TPHs was performed as reported [23], with slight modifications. Briefly, to a mixture of 0.02 mol hydroquinone and 0.01 mol of 3-methyl-2-buten-1-ol or geraniol or farnesol or phytol or geranylgeraniol in 25 mL of anhydrous Et_2O were added 2 mL of $BF_3 \cdot Et_2O$. The mixture was stirred for 3 h at room temperature (RT). After adding H_2O, the solution was extracted with Et_2O, and next, the organic extract was chromatographed on a silica gel column with a gradient of petroleum ether-Et_2O as eluent. The purified prenylhydroquinones (PHs) were identified by comparison of their spectral data (NMR) reported in literature [23]. The purified PHs were submitted to oxidation of hydroquinone ring by reaction with Ag_2O. After oxidation step that make able the hydroquinone ring to be more reactive towards the substitution mainly in position 3′ and less in 4′, thiosalicylic acid dissolved in ethanol was added to the solutions of PHs and stirred for 5 min at RT. After evaporation of solvent, **TPH** compounds were purified by silica gel column chromatography eluted with a gradient of petroleum ether-Et_2O. The synthesis of **TAVA** was performed as reported [54].

*4.1.1. NMR data for compounds **TPH1-5***

^1H and ^{13}C NMR spectra were recorded at 600.13 MHz on a Bruker DRX-600 spectrometer, equipped with a TCI Cryo Probe TM,

fitted with a gradient along the Z axis and on Bruker instruments at 400 MHz. Samples for NMR analysis were dissolved in the appropriate solvent ($CDCl_3$); a downfield shift of the signal of the solvent was used as the internal standard.

*4.1.1.1. 2-[2,5-Dihydroxy-3-(3-methylbut-2-enyl)phenylthio]benzoic acid (**TPH1**).* ^{1}H NMR δ: 9.95 (1H), 7.93 (1H), 7.41 (1H), 7.39 (1H), 7.21 (1H) 6.95 (1H), 6.85 (2H), 5.71 (1H), 4.42 (1H), 3.95 (1H), 3.48 (2H), 1.69 (3H), 1.63 (3H); ^{13}C NMR δ: 169.4, 150.8, 137.2, 134.6, 148.3, 131.4, 131.0, 132.1, 130.9, 129.3, 127.2, 123.6, 116.9, 116.1, 113.5, 28.9, 25.8, 17.5.

*4.1.1.2. (E)-2-((3-(3,7-Dimethylocta-2,6-dien-1-yl)-2,5-dihydroxyphenyl)thio)benzoic acid (**TPH2**).* ^{1}H NMR δ: 9.93 (1H), 7.91 (1H), 7.41 (1H), 7.39 (1H), 7.21 (1H), 6.62 (1H), 6.55 (1H), 6.52 (1H), 5.24 (1H), 5.0 (1H), 3.24 (2H), 2.03 (2H), 2.06 (2H), 1.70 (3H), 1.63 (3H), 1.54 (3H); ^{13}C NMR δ: 169.0, 147.7, 148.6, 148.2, 137.2, 134.6, 131.4, 131.0, 130.9, 128.1, 127.2, 123.6, 122.0, 120.8, 116.6, 116.2, 114.3, 40, 30, 26.7, 26.6, 18.1, 15.5.

*4.1.1.3. 2-((2,5-Dihydroxy-3-((2E,6E)-3,7,11-trimethyldo-deca-2,6,10-trien-1-yl)phenyl)thio)benzoic acid (**TPH3**).* ^{1}H NMR δ: 9.97 (1H), 7.93 (1H), 7.40 (1H), 7.35 (1H), 7.21 (1H), 6.61 (3H), 5.32 (1H), 5.13 (2H), 3.32 (2H), 1.77 (3H), 1.70 (3H), 1.61 (6H); ^{13}C NMR δ: 169.2, 149.4, 148.2, 138.7, 137.2, 135.6, 134.6, 131.5, 131.4, 131.0, 130.9, 128.5, 127.2, 124.5, 123.8, 121.4, 116.7, 113.8, 39.8, 29.8, 26.8, 26.5, 25.8, 17.8, 16.4, 16.2.

*4.1.1.4. 2-((2,5-Dihydroxy-3-((2E,6E,10E)-3,7,11,15-tetramethyl-hexadeca-2,6,10,14-tetraen-1-yl)phenyl)thio)benzoic acid (**TPH4**).* ^{1}H NMR δ: 9.94 (1H), 7.93 (1H), 7.42 (1H), 7.38 (1H), 7.20 (1H), 6.62 (3H), 5.32 (1H), 5.14 (2H), 5.20 (1H), 3.32 (2H), 2.00 (2H), 2.02 (2H), 1.77 (3H), 1.71 (6H), 1.70 (3H), 1.60 (6H); ^{13}C NMR δ: 169.4, 149.2, 148.0, 139.63, 138.7, 137.0, 135.6, 134.4, 132.1, 131.5, 131.2, 131.0, 130.9, 128.5, 127.2, 124.5, 123.8, 121.4, 116.7, 113.8, 39.8, 29.8, 26.8, 26.5, 25.8, 25.6, 24.3, 19.6, 17.8, 17.5, 16.2, 16.0.

*4.1.1.5. (E)-2-((2,5-Dihydroxy-3-(3,7,11,15-tetramethylhexadec-2-en-1-yl)phenyl)thio)benzoic acid (**TPH5**).* ^{1}H NMR δ: 9.95 (1H), 7.90 (1H), 7.41 (1H), 7.38 (1H), 7.21 (1H) 6.95 (1H), 6.85 (2H), 5.71 (1H), 4.42 (1H), 3.95 (1H), 3.48 (2H), 1.69 (3H), 1.63 (3H) 1.06 (6H), 1.01 (6H), 1.25 (10H); ^{13}C NMR δ: 169.1, 150.6, 148.0, 137.2, 134.4, 132.1, 131.4, 131.2, 130.9, 127.0, 129.3, 123.6, 116.9, 116.1, 113.5, 28.9, 25.8, 25.0, 24.4, 24.7, 28.2, 23.2, 33.2, 33.4, 39.9, 37.7, 37.8, 39.7, 17.5.

*4.2. Determination of EeAChE/EqBuChE inhibition (IC_{50}) by **TPHs** and **TAVA***

IC_{50}'s were determined using 0.036 U/mL of *Ee*AChE. Enzymatic activity was evaluated by the Ellman's method [24] with some modifications as described in Oset-Gasque et al., 2014 [55]. The reaction was performed in multi-well Petri dishes of 48 wells in a final volume of 500 μL. 0.036 U/mL of *Ee*AChE or eqBuChE or human BuChE (Sigma Aldrich, Madrid, Spain) in 0.1 M pH 8 phosphate buffer was incubated for 15 min at different drug concentrations at 37 °C. Afterwards, the reaction was triggered by the addition of 0.35 mM acetylthiocholine iodide (ATCh) or 0.5 mM butyrylthiocholine iodide and 0.35 mM 5,5′-ditiobis-2-nitrobenzoico (DTNB), where the DTNB produces the yellow anion 5-thio-2-nitrobenzoic acid along with the enzymatic degradation of acetylthiocholine or butyrylthiocholine. Changes in absorbance were measured at 410 nm in a Biotek PowerWave XS spectrophotometer microplate-reader. Inhibition curves were plotted by using at least nine concentrations (10nM-100μM) of each compound. IC_{50} values were calculated as the concentration of the compound yielding 50% AChE activity inhibition. Logistic curves for IC_{50} determinations were performed according to the program SigmaPlot v.11 (Systat Software INC., 2012). Data are expressed as means ± s.e.m. of at least three different experiments in triplicates.

*4.3. Kinetic analysis of the EeAChE inhibition by **TPHs** and **TAVA***

A study on the enzymatic mechanism of action of TPHs and TAVA was carried out. To obtain estimates of the Km's and Vmax's, of *Ee*AChE, reciprocal plots of 1/V versus 1/[S] were constructed at different concentrations of the substrate ATCh (0.05–1 mM) and different drug concentrations (0.01–10 μM), using the enzymatic activity assay described earlier [31]. Km's were then plotted against indicated compound concentrations, for Ki's calculations.

4.4. Neuroprotection of TPHs and TAVA

4.4.1. Cell culture and treatment

Cells from the human neuroblastoma cell line SHSY5Y were cultured in Dulbecco's: Ham's F12, 1:1 [vol/vol] containing 3.15 mg/mL glucose, 2.5 mM Glutamax, and 0.5 mM sodium pyruvate DMEM/F-12, GlutaMAX™; GIBCO, Life Technologies, Madrid (Spain), 1% Antibiotic-Antimycotic (Gibco; Life Technologies, Madrid, Spain) at 100 units of penicillin, 100 μg of streptomycin, and 0.25 μg of amphotericin B final concentrations, and supplemented with 10% Foetal Calf Serum (FCS) [Gibco; Life Technologies, Madrid (Spain)]. Cultures were seeded into flasks containing supplemented medium and maintained at 37 °C in a humidified atmosphere of 5% CO_2 and 95% air. Culture media were changed every 2 d. Cells were sub-cultured after partial digestion with 0.25% trypsin-EDTA. For assays, SHSY5Y cells were subcultured in 96-well plates at a seeding density of 2.5×10^5 cells per well. When the SHSY5Y cells reached 80% confluence, the medium was replaced with fresh medium containing 1–100 μM compounds or 0.1% DMSO as a vehicle control.

4.4.2. Measurement of cell viability

This was determined by the XTT [2,3-bis-(2-methoxy-4-nitro-5-sulfophenyl)-2*H*-tetrazolium-5-carboxanilide] method. This assay is based on the ability of living metabolically active cells to reduce the yellow tetrazolium salt (XTT) to form an orange formazan dye. Therefore, the conversion only occurs in living cells. The formazan dye formed is directly quantified using a scanning multi-well spectrophotometer at wavelength 492 nm (reference wavelength 690 nm). The amount of orange formazan formed, as monitored by its absorbance, directly correlates with the number of living cells. Control and treated neuroblastoma cells were washed with PBS and incubated with the XTT solution (final concentration 0.3 mg/mL) according to the Kit specifications. After this incubation period, orange dye solution was spectrophotometrically quantified. Results are expressed as percentages with respect to the control cells.

4.4.3. Assessment of cell viability after exposure of cell cultures to oligomycin A-Rotenone (OR) and okadaic acid (OKA) treatments

To investigate the neuroprotective effect of synthesized compounds, several concentrations of these compounds between 0.01 and 100 μM were used. Neuroprotection was assayed by measuring the increase in cell viability after 24 h treatment with a mixture of 30 μM rotenone and 10 μM Oligomycin-A (OR) or 20 nM okadaic acid (OKA), which induced neuronal cell death. The mixture of Oligomycin-A plus rotenone blocks mitochondrial electron transport chain complexes V and I, respectively, thus inducing cell death by oxidative stress, and OKA actívate tau-phosphorylation [56]. Measurements were carried out on human neuroblastoma cells SHSY5Y seeded into 96-well culture plates as described [28].

Briefly, control and treated SHSY5Y neuroblastoma cells (about 5×10^5 cells/well) were incubated with the XTT solution at 0.3 mg/mL final concentration for 3 h in a humidified incubator at 37 °C with 5% CO_2 and 95% air (v/v) and the soluble orange formazan dye formed was spectrophotometrically quantified, using a Biotek PowerWave XS spectrophotometer microplate-reader at 450 nm (reference 650 nm). All XTT assays were performed in triplicate in cells of different batches. Control cells treated with DMEM alone were regarded as 100% viability. Controls containing different DMSO concentrations (0.001–1% DMSO) were performed in all assays. The curve adjustments to estimate the EC_{50} were carried out by non-linear ponderated regression analysis of minimal squared, using logistic curves f1 = min + (max-min)/(1 + (x/IC50)^(-Hillslope)).

4.4.4. Microscopy

Light microscopy was performed on a Leica DM LB2 microscope and a digital Leica DFC 320 camera (Leica Microsystems, Barcelona, Spain).

4.5. In vitro hepatotoxicity of *TPH* compounds and *TAVA* and galanthamine in HepG2 cells

4.5.1. Cell culture and treatment

The human hepatoma cell line HepG2 were cultured in DMEM, high glucose supplemented with 10% FBS 100 units/mL penicillin, and 100 μg/mL streptomycin (reagents from GIBCO, Life Technologies, Madrid, Spain). Cultures were seeded into flasks containing supplemented medium and maintained at 37 °C in a humidified atmosphere of 5% CO_2 and 95% air. Culture media were changed every 2 d. Cells were sub-cultured after partial digestion with 0.25% trypsin-EDTA. For assays, HepG2 cells were subcultured in 48-well plates at a seeding density of 1×10^5 cells per well. When the HepG2 cells reached 80% confluence, the medium was replaced with fresh medium containing 1–100 μM compounds or 0.1% DMSO as a vehicle control.

4.5.2. Measurement of cell viability

Cell viability, measured as the mitochondrial activity of living cells, was determined by quantitative colorimetric assay with XTT (Roche Sigma-Aldrich), as described above.

5. Statistical analysis

Data are shown as mean ± SEM of data obtained from at least three independent experiments from different cultures, each of which was performed in triplicates. Statistical comparisons between the different experimental conditions were performed by using one-way analysis of variance (ANOVA), followed by Holm–Sidak's post test when the analysis of variance was significant. A p-value < 0.05 was considered statistically significant.

6. Computational methods

The sequence of the *Ee*AChE, was retrieved from the publicly available sequence database www.uniprot.org (UNIPROT: O42275). Due to the high sequence identity (~66%) with both human and *Torpedo californica* AChEs, both proteins were used as templates (PDB ID: 4EY6 and 1GQR, respectively). The multiple alignment, carried out with CLUSTALW version 1.83 [35], was used to build 50 homology models with MODELLER version 9.14 [36,37]. The protein modeled spans the sequence Pro27-Thr593, while the long 440–471 insertion falling near the dimerization domain in eelAChE sequence, being irrelevant for docking purposes, was not modeled, except for residues 457–459, conserved in the templates, which are required to ensure a proper connection between the ends of the deleted sequence. Since the first 23 residues represent the signal peptide, the protein numbering adopted in the text is referred to *Ee*AChE mature form (Pro4-Thr570). The best model in term of both Modeller objective function and Dope score was selected for the subsequent step of molecular docking.

To carry out docking calculations, the starting ligand geometries were built with Ghemical 2.99.2 [38], and energy minimized at molecular mechanics level first, using Tripos 5.2 force field parametrization [39], and then at AM1 semi-empirical level.

Since the ligands differ each other for the hydrophobic pendant bound to the hydroquinone-thiosalicylic acid moiety, each ligand was broken up in the two aforementioned groups, which were independently optimized using GAMESS program [40] at the Hartree-Fock level with STO-3G basis set, followed by a single-point HF energy evaluation at the 6-31G* level to derive the partial atomic charges for the ligands by the RESP procedure [41].

Docking studies were performed with AutoDock 4.2 [37] and AutoDockVina 1.1.2 [42]. The *Ee*AChE model and the ligands were processed with AutoDock Tools (ADT) package version 1.5.6rc1 [37] to merge non polar hydrogens, calculate Gasteiger charges and select rotatable sidechain bonds. 22.5 × 22.5 × 22.5 Å grids with a spacing of 0.375 Å and centered in the catalytic anionic site (CAS), were generated with the program AutoGrid 4.2 included in Autodock 4.2 distribution and used for the docking step. Docking runs were carried out both by keeping the protein fixed and by allowing the rotation of Tyr123(hAChe Y124), Tyr332(hAChE Y337) and Tyr336 (hAChE Y341). 100 molecular AutoDock docking runs for each docking calculation were performed adopting a Lamarckian Genetic Algorithm (LGA) and the following associated parameters: 100 individuals in a population with a maximum of 15 million energy evaluations and a maximum of 37,000 generations, followed by 300 iterations of Solis and Wets local search. Flexibility was used for all rotatable bonds of both docked ligands. For each docking run from both AutoDock and AutoDockVina, the poses were subjected to visual inspection and those exhibiting the lowest predicted AutoDock binding free energy and forming direct interactions with the residues critical for AChE catalytic process were selected for the subsequent MD simulations of ligand- *Ee*AChE complexes.

The selected complexes from docking calculations were completed by addition of all hydrogen atoms and underwent EM and then MD simulations with Amber12 pmemd.cuda module [43,44], using the ff12SB version of AMBER force field [45] for the protein and gaff parameters [46] for the ligands.

To perform molecular dynamics (MD) simulation in solvent, complexes were confined in TIP3P water periodic boxes exhibiting a minimum distance between solute and box surfaces of 10 Å, using the tleap module of AmberTools13 program [47]. Each system was then neutralized by addition of counterions (Na+) and underwent 1000 steps of EM with solute atoms harmonically restrained to their starting positions using a force constant of 10 kcal mol-1Å-1. The resulting structures were submitted to 90 ps restrained MD (5 kcal mol-1Å-1) at constant volume, gradually heating the system to 300 K, followed by 60 ps restrained MD (5 kcal mol-1Å-1) at constant temperature (300 K) and pressure (1 atm) to adjust system density. Production MD simulations were carried out at constant temperature (300 K) and pressure (1 atm) for 20 ns with a time-step of 2 fs. Bonds involving hydrogens were constrained using the SHAKE algorithm [48]. Visual inspection and graphical analysis were performed with VMD 1.9.2 [49] and UCSF Chimera 1.10.1 [50], the last program was also used to draw the figures.

Author contribution

G.T. conceived the synthesis and synthesized compounds and

wrote the manuscript; N.G-F carried out the biochemical and pharmacological experiments. B.P, and C.I. assisted in the synthesis and characterization of compounds. R.M.V. conceived and carried out the molecular modeling studies and wrote the manuscript. S.C., assessed in the kinetic analysis of enzyme inhibition. J.M.-C. helps in the correction of the manuscript. M.J.O.G. planned, carried out, analyzed and supervised the biochemical and pharmacological experiments and wrote the manuscript.

Acknowledgments

MJOG thanks MINECO (Spain) for grant SAF2010-20337, and UCM for grant GR3/14. JMC thanks MINECO (Spain) (SAF2012-33304 and SAF2015-56685-R). for continued support. This work was partially supported by the International Program "Short Term Mobility (S.T.M.)" of CNR—National Research Council of Italy.

References

[1] R.J. Castellani, R.K. Rolston, M.A. Smith, Alzheimer disease, Disease-a-Month 56 (9) (2010) 484–546.
[2] C. Reitz, C. Brayne, R. Mayeux, Epidemiology of Alzheimer disease, Nat. Rev. Neurol. 7 (3) (2011) 137–152.
[3] M. Goedert, M.G. Spillantini, A century of Alzheimer's disease, Science 314 (5800) (2006) 777–781.
[4] R.D. Terry, N.K. Gonatas, M. Weiss, Ultrastructural studies in Alzheimer's presenile dementia, Ann. J. Pathol. 44 (1964) 269–297.
[5] I. Grundke-Iqbal, K. Iqbal, Y.C. Tung, M. Quinlan, H.M. Wisniewski, L.I. Binder, Abnormal phosphorylation of the microtubule-associated protein tau (tau) in Alzheimer cytoskeletal pathology, Proc. Natl. Acad. Sci. U. S. A. 93 (13) (1986) 4913–4917.
[6] M. Rosini, E. Simoni, A. Milelli, A. Minarini, C. Melchiorre, Oxidative stress in Alzheimer's disease: are we connecting the dots? J. Med. Chem. 57 (7) (2014) 2821–2831.
[7] E.K. Perry, B.E. Tomlinson, G. Blesseed, K. Bergmann, P.H. Gibson, R.H. Perry, Correlation of cholinergic abnormalities with senile plaques and mental test scores in senile dementia, Br. Med. J. 2 (6150) (1978) 1457–1459.
[8] V.N. Talesa, Acetylcholinesterase in Alzheimer's disease, Mech. Ageing Dev. 122 (16) (2001) 1961–1969.
[9] A.V. Terry, J.J. Buccafusco, C. Wilson, Cognitive dysfunction in neuropsychiatric disorders: selected serotonin receptor subtypes as therapeutic targets, Behav. Brain Res. 195 (1) (2008) 30–38.
[10] T. Gura, Hope in Alzheimer's fight emerges from unexpected places, Nat. Med. 14 (9) (2008) 894.
[11] M. Racchi, M. Mazzucchelli, E. Porrello, C. Lanni, S. Govoni, Acetylcholinesterase inhibitors: novel activities of old molecules, Pharmacol. Res. 50 (4) (2004) 441–451.
[12] R. León, A.G. García, J. Marco-Contelles, Recent advances in the multitarget-directed ligands approach for the treatment of Alzheimer's disease, Med. Res. Rev. 33 (1) (2013) 139–189.
[13] L. Minale, R. Riccio, S. Sodano, Avarol a novel sesquiterpenoid hydroquinone with a rearranged drimane skeleton from the sponge, Tetrahedron Lett. 15 (38) (1974) 3401–3404.
[14] S. De Rosa, Mediterranean marine organisms as source of new potential drugs, in: A.P. Rauter, F.B. Palma, J. Justino, M.E. Araujo, S.P. dos Santos (Eds.), Natural Products in the New Millennium: Prospects and Industrial Application, Kluwer Academic Publishers, Dordrecht, 2002, pp. 441–461.
[15] S. De Rosa, A. De Giulio, G. Strazzullo, Biologically active metabolites from marine organisms and some semi-synthetic derivatives, Trends Org. Chem. 2 (1991) 127–141.
[16] M.J. Gašić, Biologically active compounds from marine sponges: an approach to chemical and biochemical characterization of the avarol/avarone redox couple, J. Serb. Chem. Soc. 53 (1988) 229–249.
[17] B. Pejin, C. Iodice, G. Tommonaro, S. De Rosa, Synthesis and biological activities of thio-avarol derivatives, J. Nat. Prod. 71 (2008) 1850–1853.
[18] G. Tommonaro, B. Pejin, C. Iodice, A. Tafuto, S. De Rosa, Further in vitro biological activity evaluation of amino-, thio- and ester- derivatives of avarol, J. Enz. Inhib. Med. Chem. 30 (2) (2014) 1–3.
[19] S. De Rosa, G. Tommonaro, Bioactive marine prenylated quinones/quinols, in: Atta-Ur-Rahaman (Ed.), Studies in Natural Products Chemistry (Bioactive Natural Products) 36, Elsevier Science Publishers- Amsterdam, 2012, pp. 163–211. Chap. 6.
[20] B. Pejin, C. Iodice, V. Kojic, D. Jakimov, M. Lazovic, G. Tommonaro, In vitro evaluation of cytotoxic and mutagenic activity of avarol, Nat. Prod. Res. (2015), http://dx.doi.org/10.1080/14786419.2015.1052067.
[21] B. Pejin, A. Ciric, D. Markovic, G. Tommonaro, M. Sokovic, In vitro avarol does affect the growth of *Candida* sp, Nat. Prod. Res. (2015), http://dx.doi.org/10.1080/14786419.2015.1091454.
[22] T. Bozić, I. Novaković, M.J. Gasić, Z. Juranić, T. Stanojković, S.C. Tufegdzić, Z. Kljajić, D. Sladić, Synthesis and biological activity of derivatives of the marine quinone avarone, Eur. J. Med. Chem. 45 (2010) 923–929.
[23] S. De Rosa, A. De Giulio, C. Iodice, Biological effects of prenylated hydroquinones: structure-activity relationships studies in antimicrobial, brine shrimp, and fish lethality assays, J. Nat. Prod. 12 (1994) 1711–1716.
[24] G.L. Ellman, K.D. Courtney, B.J. Andres, R.M. Featherstone, A new and rapid colorimetric determination of acetylcholinesterase activity, Biochem. Pharmacol. 7 (1961) 88–90.
[25] A. Romero, J. Egea, A.G. García, M.G. López, Synergistic neuroprotective effect of combined low concentrations of galantamine and melatonin against oxidative stress in SH-SY5Y neuroblastoma cells, J. Pineal Res. 49 (2010) 141–148.
[26] J.P. Lopes, G. Tarozzo, A. Reggiani, D. Piomelli, A. Cavalli, Galantamine potentiates the neuroprotective effect of memantine against NMDA-induced excitotoxicity, Brain Behav. 3 (2013) 67–74.
[27] L. Del Barrio, M.D. Martín-de-Saavedra, A. Romero, E. Parada, J. Egea, J. Avila, J.M. McIntosh, S. Wonnacott, M.G. López, Neurotoxicity induced by okadaic acid in the human neuroblastoma SH-SY5Y line can be differentially prevented by α7 and β2* nicotinic stimulation, Toxicol. Sci. 123 (2011) 193–205.
[28] R. Kumar, A. Nordberg, T. Darreh-Shori, Amyloid-β peptides act as allosteric modulators of cholinergic signalling through formation of soluble BAβACs, Brain 139 (2016) 174–192.
[29] N.C. Inestrosa, A. Álvarez, C.A. Pérez, R.D. Moreno, M. Vicente, C. Linker, O.I. Casanueva, C. Soto, J. Garrido, Acetylcholinestearse accelerates assembly of amyloid-beta-peptides into Alzheimer's fibrils: possible role of the peripheral site of the enzyme, Neuron 16 (1996) 881–891.
[30] M. Chioua, J. Pérez-Peña, N. García-Font, I. Moraleda, I. Iriepa, E. Soriano, J. Marco-Contelles, M.J. Oset-Gasque, Pyranopyrazolotacrines as non neurotoxic, Aβ-anti-aggregating and neuroprotective agents for Alzheimer's disease, Future Med. Chem. 7 (2015) 845–855.
[31] M. Esquivias-Pérez, E. Maalej, A. Romero, F. Chabchoub, A. Samadi, J. Marco-Contelles, M.J. Oset-Gasque, Nontoxic and neuroprotective β-naphthotacrines for Alzheimer's disease, Chem. Res. Toxicol. 26 (2013) 986–992.
[32] S. Wilkening, F. Stahl, A. Bader, Comparison of primary human hepatocytes and hepatoma cell line HepG2 with regard to their biotransformation properties, Drug Metab. Dispos. 31 (2003) 1035–1042.
[33] R.A. Osseni, C. Debbasch, M.O. Christen, P. Rat, J.M. Warnet, Tacrine-induced reactive oxygen species in a human liver cell line: the role of anethole dithiolethione as a scavenger, Toxicol. In Vitro 13 (1999) 683–688.
[34] M. Rosini, E. Simoni, A. Milelli, A. Minarini, C. Melchiorre, Oxidative stress in Alzheimer's disease: are we connecting the dots? J. Med. Chem. 57 (2014) 2821–2831.
[35] J.D. Thompson, D.G. Higgins, T.J. Gibson, CLUSTAL W: improving the sensitivity of progressive multiple sequence alignment through sequence weighting, position-specific gap penalties and weight matrix choice, Nucleic Acids Res. 22 (1994) 4673–4680.
[36] A. Sali, T.L. Blundell, Comparative protein modelling by satisfaction of spatial restraints, J. Mol. Biol. 234 (1993) 779–815, http://dx.doi.org/10.1006/jmbi.1993.1626.
[37] G.M. Morris, R. Huey, W. Lindstrom, M.F. Sanner, R.K. Belew, D.S. Goodsell, et al., AutoDock4 and AutoDockTools4: automated docking with selective receptor flexibility, J. Comput. Chem. 30 (2009) 2785–2791.
[38] T. Hassinen, M. Peräkylä, New energy terms for reduced protein models implemented in an off-lattice force field, J. Comput. Chem. 22 (2001) 1229–1242.
[39] M. Clark, R.D. Cramer, N. Van Opdenbosch, Validation of the general purpose tripos 5.2 force field, J. Comput. Chem. 10 (1989) 982–1012.
[40] M.W. Schmidt, K.K. Baldridge, J.A. Boatz, S.T. Elbert, M.S. Gordon, J.H. Jensen, et al., General atomic and molecular electronic structure system, J. Comput. Chem. 14 (1993) 1347–1363.
[41] T. Fox, P.A. Kollman, Application of the RESP methodology in the parametrization of organic solvents, J. Phys. Chem. B 102 (1998) 8070–8079.
[42] O. Trott, A.J. Olson, Software news and update AutoDock Vina: improving the speed and accuracy of docking with a new scoring function, efficient optimization, and multithreading, J. Comput. Chem. 31 (2010) 455–461.
[43] A.W. Götz, M.J. Williamson, D. Xu, D. Poole, S. Le Grand, R.C. Walker, Routine microsecond molecular dynamics simulations with AMBER on GPUs. 1. Generalized Born, J. Chem. Theory Comput. 8 (2012) 1542–1555.
[44] R. Salomon-Ferrer, A.W. Götz, D. Poole, S. Le Grand, R.C. Walker, Routine Microsecond Molecular Dynamics Simulations with AMBER on GPUs. 2. Explicit solvent particle mesh Ewald, J. Chem. Theory Comput. 9 (2013) 3878–3888.
[45] D.A. Case, T.A. Darden, T.E. Cheatham III, C.L. Simmerling, J. Wang, R.E. Duke, et al., AMBER 12, University of California, San Francisco, 2012.
[46] J. Wang, R.M. Wolf, J.W. Caldwell, P.A. Kollman, D.A. Case, Development and testing of a general amber force field, J. Comput. Chem. 25 (2004) 1157–1174.
[47] D.A. Case, T.A. Darden, T.E. Cheatham III, C.L. Simmerling, J. Wang, R.E. Duke, et al., AMBER 13, University of California, San Francisco, 2012.
[48] J.-P. Ryckaert, G. Ciccotti, H.J. Berendsen, Numerical integration of the cartesian equations of motion of a system with constraints: molecular dynamics of n-alkanes, J. Comput. Phys. 23 (1977) 327–341.
[49] W. Humphrey, A. Dalke, K. Schulten, VMD: visual molecular dynamics, J. Mol. Graph 14 (1996) 33–38.
[50] E.F. Pettersen, T.D. Goddard, C.C. Huang, G.S. Couch, D.M. Greenblatt, E.C. Meng, et al., UCSF Chimera—a visualization system for exploratory

research and analysis, J. Comput. Chem. 25 (2004) 1605–1612.
[51] F. Zemek, L. Drtinova, E. Nepovimova, V. Sepsova, J. Korabecny, J. Klimes, K. Kuca, Outcomes of Alzheimer's disease therapy with acetylcholinesterase inhibitors and memantine, Expert Opin. Drug Saf. 13 (2014) 759–774.
[52] Lemes LF, de Andrade Ramos G, de Oliveira AS, da Silva FM, de Castro Couto G, da Silva Boni M, Guimarães MJ, Souza IN, Bartolini M, Andrisano V, do Nascimento Nogueira PC, Silveira ER, Brand GD, Soukup O, Korábečný J, Romeiro NC, Castro NG, Bolognesi ML, Romeiro LA, Cardanol-derived AChE inhibitors: towards the development of dual binding derivatives for Alzheimer's disease. Eur. J. Med. Chem. 108 (2016) 687–700.
[53] Nepovimova E1, E. Uliassi, J. Korabecny, L.E. Peña-Altamira, S. Samez, A. Pesaresi, G.E. Garcia, M. Bartolini, V. Andrisano, C. Bergamini, R. Fato, D. Lamba, M. Roberti, K. Kuca, B. Monti, M.L. Bolognesi, Multitarget drug design strategy: quinone-tacrine hybrids designed to block amyloid-β aggregation and to exert anticholinesterase and antioxidant effects, J. Med. Chem. 57 (2014) 8576–8589.
[54] M.A. Amigò, M.C. Terencio, M. Payà, C. Iodice, S. De Rosa, Synthesis and evaluation of diverse thioavarol derivatives as potential UVB photoprotective candidates, Bioorgan. Med. Chem. Lett. 17 (2007) 2561–2565.
[55] M.J. Oset-Gasque, M.P. González, J. Pérez-Peña, N. García-Font, A. Romero, J. del Pino, E. Ramos, D. Hadjipavlou-Litina, E. Soriano, M. Chioua, A. Samadi, D.S. Raghuvanshi, K.N. Singh, J. Marco-Contelles, Toxicological and pharmacological evaluation, antioxidant, ADMET and molecular modeling of selected racemic chromenotacrines {11-amino-12-aryl-8,9,10,12-tetrahydro-7H-chromeno[2,3-b]quinolin-3-ols} for the potential prevention and treatment of Alzheimer's disease, Eur. J. Med. Chem. 74 (2014) 491–501.
[56] N. García-Font, H. Hayour, A. Belfaitah, J. Pedraz-Cuesta, I. Moraleda, I. Iriepa, A. Bouraiou, M. Chioua, J. Marco-Contelles, M.J. Oset-Gasque, Non-hepatotoxic, potent anticholinesterasic and neuroprotective pyranotacrines as inhibitors of beta-amyloid aggregation, oxidative stress and tau-phosphorylation for Alzheimer's disease, Eur. J. Med. Chem. 118 (2016) 178–192.